NANOMATERIALS

Structural transitions and guest/host complexing of liquid crystal helical nanofilaments induced by nanoconfinement

Hanim Kim,[1] Seong Ho Ryu,[1] Michael Tuchband,[2] Tae Joo Shin,[3] Eva Korblova,[4] David M. Walba,[4] Noel A. Clark,[2] Dong Ki Yoon[1]*

A lamellar liquid crystal (LC) phase of certain bent-core mesogenic molecules can be grown in a manner that generates a single chiral helical nanofilament in each of the cylindrical nanopores of an anodic aluminum oxide (AAO) membrane. By introducing guest molecules into the resulting composite chiral nanochannels, we explore the structures and functionality of the ordered guest/host LC complex, verifying the smectic-like positional order of the fluidic nematic LC phase, which is obtained by the combination of the LC organization and the nanoporous AAO superstructure. The guest nematic LC 4′-*n*-pentyl-4-cyanobiphenyl is found to form a distinctive fluid layered ordered LC complex at the nanofilament/guest interface with the host 1,3-phenylene bis[4-(4-nonyloxyphenyliminomethyl)benzoate], where this interface contacts the AAO cylinder wall. Filament growth form is strongly influenced by mixture parameters and pore dimensions.

INTRODUCTION

A variety of bent mesogenic molecules, upon cooling a neat isotropic melt, self-organize into smectic liquid crystal (LC) phases that grow in the form of helical nanofilaments (HNFs), which are precisely structured bundles of twisted layers, ~30 nm in diameter and of macroscopic length, stabilized by saddle-splay layer curvature (*1*–*5*). These filaments then pack together like spaghetti in a box, filling space with spontaneously homochiral nanoporous arrays (*6*). Novel hierarchical self-assemblies can be achieved by incorporating the melt into a nanostructured host under conditions of additional nanoconfinement. For example, cooling the LC in the cylindrical nanoscale pores of anodic aluminum oxide (AAO) membrane results in hierarchical composite nanoporous systems, in which each AAO nanochannel can hold a single chiral LC nanofilament (*7*, *8*). This demonstration of hierarchical LC/AAO supramolecular organization suggested a new platform for fabrication of multicomponent composite systems that obtain functionality from the combination of self-assembled LC organization and nanoporous AAO superstructure.

Liquid-phase applications such as chemical catalysis or chiral separations would require additional fluid components in the channels. Here, we investigate the effects of the addition of a guest nematic LC component into these hierarchical LC/AAO assemblies, with the goal of exploring its interactions with the bent cores and AAO cylindrical nanopores. This can also be considered a general approach to explore the role of confinement of nematic LCs, as it provides strong anchoring at the nanoscale in a three-dimensional (3D) system using template-assisted nanoconfinement. This is well known to be one of the most effective ways to control small–molecular weight soft materials by inducing a spatial compartmentalization through intermolecular segregation (*9*–*12*).

[1]Graduate School of Nanoscience and Technology, Korea Advanced Institute of Science and Technology, Daejeon 34141, Republic of Korea. [2]Department of Physics and Soft Materials Research Center, University of Colorado, Boulder, CO 80309, USA. [3]Ulsan National Institute of Science and Technology (UNIST) Central Research Facilities & School of Natural Science, UNIST, Ulsan 689-798, Republic of Korea. [4]Department of Chemistry and Soft Materials Research Center, University of Colorado, Boulder, CO 80309, USA.
*Corresponding author. Email: nandk@kaist.ac.kr

To implement this strategy, we mixed a prototypical rod-like LC mesogen 4′-*n*-pentyl-4-cyanobiphenyl (5CB) with a prototypical bent-core mesogen 1,3-phenylene bis[4-(4-nonyloxyphenyliminomethyl) benzoate] (NOBOW) (*1*–*5*), and the mixtures were loaded into porous AAO nanochannels having a specific diameter of d_{AAO} = 60 nm and length of L = 5 μm, as illustrated in Fig. 1 (details are described in Materials and Methods). For the present study, a 50:50 (w/w) mixture was chosen to study the nematic LC ordering in the confined system based on weight ratio variation experiments in bulk and nanoconfined geometries (fig. S1 to S3).

RESULTS

To investigate the molecular orientational order of the tightly confined 5CB phase of these samples, we performed grazing incidence x-ray diffraction (GIXD) experiments (Fig. 1 and fig. S4). The details in structural changes during the thermal phase transition were investigated by in situ GIXD experiments upon cooling (Fig. 2). We focused on the small-angle region to determine the interlayer information of 5CB/NOBOW mixture in 2D and its circular averaged 1D data (Fig. 2, B and C) compared to the neat NOBOW case (Fig. 2A) (*7*). This approach enabled the determination of the in-plane and out-of-plane nanostructure of the HNF and LC ordering in the AAO nanochannels, as follows.

GIXD results for neat NOBOW

As reported in the previous study, neat NOBOW follows a fundamental mechanism to form HNFs (known as B4) via saddle-splay deformation of initial polar-tilted smectic layers (defined as B2) in the confined geometries (*7*, *8*). The initial phase transition, iso-to B2 smectic layering (q_{B2} = 1.65 nm^{-1}) of the neat NOBOW, first appeared at $\chi \approx 0°$ (χ denotes the angular variation from the helical axis z), indicating that the layer normal vector, s, was parallel to the channel axis, z (Fig. 1C) (*7*). Then, NOBOW molecules could self-assemble into single HNF oriented parallel to the AAO nanochannels (Figs. 2 and 3, and fig. S2) (*7*), which was confirmed by the diagonal peaks corresponding to the layer spacing in the NOBOW HNF phase ($q_{HNF} \approx$ 1.3 nm^{-1}, lamellar spacing $d \approx$ 4.48 nm; Fig. 1, B and C, blue lines).

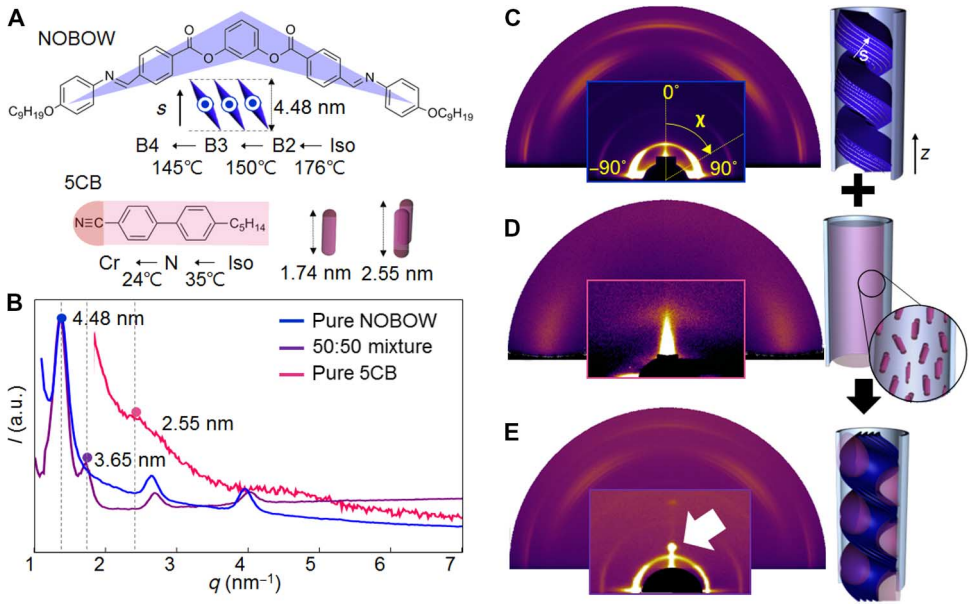

Fig. 1. Material information and GIXD investigation showing the perfectly controlled 5CB molecules guided along the helical geometries of the prealigned HNFs in the nanoconfined geometries (d_{AAO} = 60 nm, L = 5 mm). (**A**) Molecular configurations of 5CB and NOBOW. (**B**) 1D GIXD spectrum that provides the quantitative information of interlayering and clustering for the confined NOBOW and 5CB in the small-angle region. a.u., arbitrary units. (**C** to **E**) 2D GIXD patterns acquired from pure NOBOW (blue line) (C), pure 5CB (pink line) (D), and their 50 wt % mixtures (purple line) (E) with the model sketches of each system.

Although the HNFs are well oriented along the nanochannel axis (Fig. 3), there is a broad angular distribution of the lamellar and in-layer reflections, a result of the highly twisted layer structure of the HNFs (Figs. 1C and 2A).

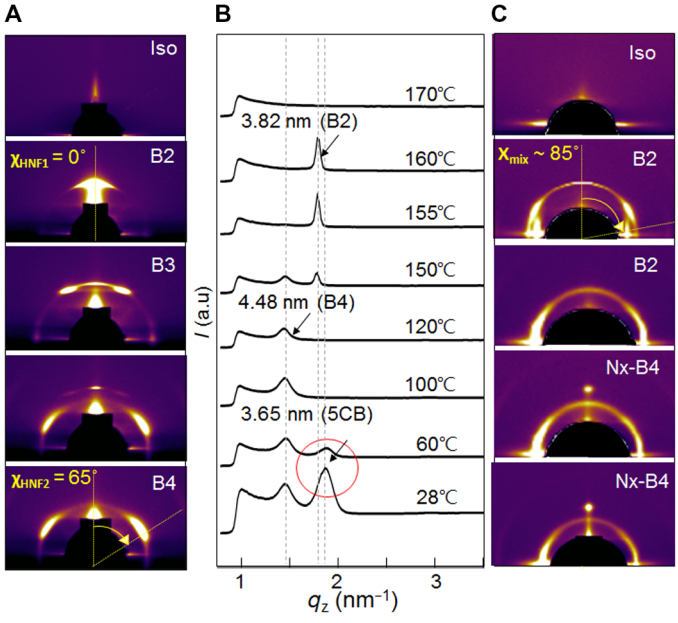

Fig. 2. In situ GIXD analysis tracing the thermal history of the 5CB-NOBOW 50:50 mixture in AAO upon cooling (d_{AAO} = 60 nm). (**A**) Acquired 2D in situ GIXD images of neat NOBOW. (**B**) 1D vertical linecut for the 50 wt % mixture in the q range of 0.6 to 3.5 nm^{-1}, showing the evolution of the 2D diffraction peaks from the mixture and the 2D diffraction pattern. (**C**) In situ GIXD images of the 50:50 mixture of 5CB/NOBOW.

GIXD results for neat 5CB

Figure 1D shows the GIXD result from channels filled with pure 5CB. In this case, the planar alignment of 5CB on the cylindrical nanochannel wall produced a strong alignment of its nematic director to be parallel to the cylinder axis, because this orientation eliminates nematic director distortion due to wall curvature (*13*–*16*). The oriented nematic director that exhibits a diffuse peak at a small angle represented the typical dimension for a 5CB dimer in the pure 5CB nematic phase ($q_N \approx 2.45$ nm^{-1}, layer spacing $d \approx 2.55$ nm; Fig. 1, A, B, and D, pink lines) (*17*, *18*). Here, the "diffuse" peak (Fig. 1D) was caused by end-to-end molecular interactions in the nematic LC. These interactions were rarely observed in the normal nematic LCs prepared in bulk because of the highly fluid behavior of the 5CB molecules. The wide-angle, in-plane arc peak represented the nearest-neighbor "sideways" interaction of the 5CB molecules and indicated the orientation of the director along the nanochannel long axis (described in Fig. 1D).

GIXD results for NOBOW/5CB mixtures

Several new features appear in the GIXD for the 50:50 5CB/NOBOW mixture upon cooling in the nanochannels. The sequential phase transition behavior of the binary mixture of 5CB/HNFs (*19*–*22*) is quite different from the neat NOBOW in Fig. 2A, as shown in the 2D diffraction patterns (Fig. 1, B and E, purple lines). The initial B2 layer peak for the mixture was observed at the azimuthal angle position of χ = 80° to 85° (Fig. 2C). This indicates a nearly vertical alignment of initial layers, which is totally opposite to the neat NOBOW case. Once B2-to-B4 transition occurred at the temperature range of 145° to 150°C, the B4-twisted layer diffraction peak at $q_{HNF} = 1.3$ nm^{-1} appeared for both the neat NOBOW and the 5CB-mixed NOBOW. The 2D diffraction pattern coming from the HNFs has lamellar and in-plane reflections at values of q similar to those of neat NOBOW. This

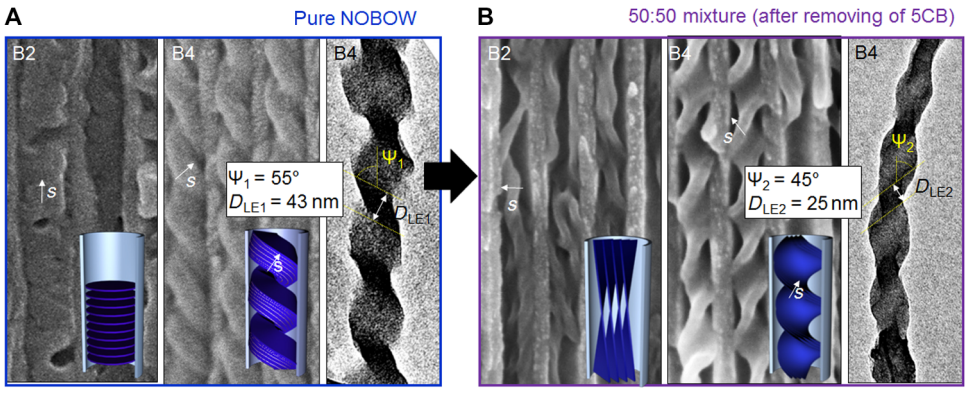

Fig. 3. Comparison of the host templating HNF morphologies using SEM and TEM methods. (**A**) Pure NOBOW and (**B**) the NOBOW-5CB 50:50 mixture after selective removal of 5CB in EtOH. Schematic illustrations are included in the inset images for the nanoconfined binary mixture of 5CB/NOBOW.

observation is consistent with previous observations of NOBOW/calamitic LC mixtures showing that a guest-like 5CB should be insoluble within the filament and expelled from the HNF to the interstitial space between the HNF and the AAO nanochannel wall (*19*–*21*). However, the GIXD of the mixture shows rather different angular distributions from those of neat NOBOW, indicating some difference in the HNF superstructure when grown from the confined mixture (Fig. 1, C and E). At temperature $T \sim 60°C$, an additional reflection appears, giving the strong spot at $\chi = 0°$ in the azimuthal orientation (Fig. 1E, white arrow). This peak appears parallel to the axis of the cylindrical AAO nanopores at $q_{mix} \approx 1.7\ nm^{-1}$, corresponding to a spacing of ~3.65 nm (Fig. 1B, purple line). This spacing has no known correspondence for either of the neat components, not matching the diffuse peak position for the 5CB dimer, for example, ~2.55 nm in Fig. 1B (pink line) or any lamellar reflection of NOBOW in any of its phases. In particular, the expelled 5CB molecules must exist as an isotropic melt state in this temperature range. However, this additional reflection exhibits an exceptionally high degree of orientational order (Figs. 1E and 2C). Considering the broad mosaic distributions of the layer ordering in the HNFs, it therefore appears certain that the source of this new reflection is not within the HNFs. The only rationale for obtaining this strong orientational ordering within the pores is the nematic alignment from coexisting 5CB by the curved nanochannel walls. Considering the absence of assignable spacing in either of the components and the expulsion of 5CB from the HNF interior, we are therefore led to seek conditions in the nanochannels such that specific interactions between the 5CB and NOBOW molecules could form a complexed state not only at the interface between the HNF and expelled 5CB but also in close proximity to the AAO nanocylinder wall. Under this limited spatial condition, 5CB could produce a highly oriented LC state with distinctive 1D layer ordering, appearing as the center spot at $\chi = 0°$. This behavior will be further discussed below.

Morphological comparison by EM observation

To clarify the different phase evolutions for each case, we performed electron microscopy (EM) observation, giving us the additional experimental grounds for the morphological changes at all phase sequences. The morphological transitions at the B2 and B4 phases of the HNF template were directly visualized by the sudden quenching method (see Materials and Methods). Note that the nematic phase of the 5CB molecule was in a fluidic liquid state at room temperature and was susceptible to the electron beam of EM even under vacuum conditions. Therefore, only the remaining backbone structure of the B2 and B4 phases of the NOBOW molecules were observed after selective removal of the 5CB molecules using ethanol (EtOH), in which the remaining B2 smectic layers and the B4 HNF could directly reflect the collective behavior of 5CB; the solvent resistances of the HNF morphologies in EtOH were verified (fig. S5). All the EM samples were gathered by cross-sectioning the samples in porous AAO films after quenching from each phase temperature at room temperature (see Materials and Methods). A scanning EM (SEM) image at the B2 smectic phase of neat NOBOW showed that the layer normal vector, *s*, was aligned parallel with the channel axis, *z*, to form disc-like structures (Fig. 3A), as expected from the GIXD results (Fig. 2A). This resulted from the planar-anchored NOBOW molecules with the inner surface of the AAO channels (*7*). A further cooling process induced the B4 phase and followed the basic principles of the pure NOBOW (*1*, *7*). A transmission EM (TEM) image of the HNF showed the layered structures of the resulting HNFs with a specific layer-twisting angle, Ψ, with respect to *z* ($\Psi \approx 55°$).

As shown in Fig. 3, the pure NOBOW (Fig. 3A) and the mixture of 5CB/NOBOW (Fig. 3B) also differed in their morphologies over the whole phase transitions, for example, *s* was perpendicular to *z* in the mixture (Fig. 3B), which was consistent with the GIXD results (Fig. 2C). This was due to the different interfacial condition under the coexistence of 5CB molecules. Contact angle measurements (fig. S6, measured at the isotropic melt state for each case) showed that 5CB has higher surface affinity to the inner surface of the AAO nanochannels than NOBOW molecules. Under this condition, 5CB molecules mostly place between the pretransitioned HNFs and the inner surface of the channels when confined in AAO as the mixture, acting as a lubricant between the oxide wall and the NOBOW materials. The presence of 5CB changed the boundary condition for NOBOW molecules in the channels, minimizing the surface anchoring between NOBOW and the inner AAO channel wall. Upon cooling, the NOBOW molecules started to form initial B2 smectic layers along the channel geometry in a direction parallel to the channel (Figs. 2C and 3B), and these different molecular arrangements of the mixtures in the B2 phase further influenced the HNF formation.

DISCUSSION

Pure HNFs normally show tip-splitting growth as the basic morphological evolution at bulk state (*1*, *2*, *7*). The principal growth mode of the HNF phase was that of layers propagating from the tip or

branching to another filament rather than randomly nucleating within the pores. However, neat NOBOW molecules have a much lower thermal conductivity (κ ≈ 0.15 W/mK) than Al_2O_3 (κ ≈ 30 W/mK) in the confined geometries, such as AAO (*23*), making the AAO film nearly isothermal in the temperature gradient along the pore direction. In this case, the HNFs only grew along the vertical channel direction by the thermal gradient from the top of the channels, excluding the tip-splitting process.

In contrast, in the case of binary mixture, the coexisting isotropic 5CB molecules occupied the interstitial volume between the oxide wall and the HNF, which changed the growth mode of the pretransition of HNFs: At high temperatures (above 185°C), both components were in the isotropic fluid state. Once the system was cooled down to iso-to-B2 transition, nearly 100% of NOBOW grew in the initial layers along the channel, which was a process of displacement of the components in the direction normal to the channel axis. In a given length of channel, the final state had nearly all the NOBOW in the filaments and all the 5CB in the surrounding volume. Under these conditions, because the diffusive unmixing of the components takes some time, the filament must grow along both the pore axis and radially. There was still some NOBOW in growing out of central filaments in the isotropic phase, and this NOBOW further attached to the filament surface. During this process, the filament grew not only in the vertical direction but also in diameter, eventually encountering the solid surface of the AAO pore. As the B2-to-B4 transition was approached, the local layer orientation at a given place in the HNF was obtained by twisting the local layers with the twisting angle of ~45° to the pore axis, in which the value is similar to the bulk HNFs (*1*, *2*, *5*) because of the coexistence of isotropic 5CB minimizing the surface anchoring from the AAO wall. At the low temperature range (below 60°C), coexisting 5CB molecules started to align along the layer-twisting direction of preformed HNF backbone structures (*24*, *25*) confined in the interstitial volume between HNFs and the AAO wall. The arrangement of 5CB molecules was highly restricted by both the mutual interaction with NOBOW at the HNF surface and the planar surface anchoring from the AAO wall. According to some previous works, 5CB molecules could exhibit smectic-like high positional ordering very near the surface even above the T_{NI} temperature (~60°C), when 5CB molecules were in contact with two antagonistic surface boundaries: one with the planar substrates and the other one with the homeotropic air boundary (*26*–*28*). Similar to this case, for the nanoconfined 5CB/NOBOW mixture, the anchoring condition of 5CB is planar on the AAO wall and homeotropic at the 5CB/NOBOW contact zone (*29*). Under this condition, we could expect a similar layering behavior from 5CB that is anchored to the NOBOW molecules at the HNF surfaces that partially formed 5CB/NOBOW smectic A complex at the interface (Fig. 4, A and B). In addition, the interstitial volume in helical voids where the nematic 5CB molecules are confined (Fig. 4, A and B, pink area) is much smaller than the nematic correlation anchoring length ($\xi = K/W_e$; K denotes the bulk elastic constant of nematic LCs, and W_e denotes the strength of the anchoring in units of energy; normally, $K \approx 10^{-11}$ N and $W_e \approx 10^{-5}$ J/m^2 for bulk 5CB) (*30*). This situation required no director deformations for the nematic 5CB in helical voids, in which they also contribute to the exceptionally high orientational ordering of the 5CB/NOBOW complex at the AAO contact zone, appearing as the bright center spot in 2D diffraction pattern (Figs. 1E and 4B).

The boundary condition presented by the pore wall will strongly favor the orientation of the 5CB/NOBOW complex parallel to the pore axis to avoid director deformation due to the high curvature of the wall, according to the Berreman effect (*31*, *32*). As the system cools, the three components of the 5CB/NOBOW/AAO curvature combine to produce an LC state at the wall having the orientation preferred by the wall, a director along the pore axis. That is, as the surface is approached, the tilted layers of pure NOBOW give way to a mixed 5CB/NOBOW surface phase that is aligned with the director along the pore axis, according to the boundary condition. This phase happens to be smectic A–like perfect ordering appearing as a bright center peak, as shown in Fig. 1E, with an unusual layer spacing of 3.65 nm suggestive of a 5CB-dominated smectic A as the partial 5CB/NOBOW complex state at the interface. Considering this unusual value of d spacing, 5CB dimers might have the nonintercalated bilayer configuration (minimizing dipole repulsion) with the estimated period of $d \approx 2l$ (l denotes the length of 5CB, which is about 1.74 to 1.85 nm). This tendency is quite different from the general feature of bulk 4′-*n*-alkyl-4-cyanobiphenyl (NCB) materials that have $l < d < 2l$ (*17*, *18*, *33*) that is even observed in the nanoconfinement experiments for pure 5CB and 8CB (fig. S7). This result indicates that the coexisting HNFs change the interfacial anchoring condition of 5CB molecules, which induces the unusual smectic-like molecular packing. The absence of the center spot in the 40-nm nanopores also indicates that the mixed state requires a certain amount of HNF contact with the wall (fig. S8). In addition, the macroscopic chirality of the 5CB nematic director is an interesting aspect of this work, as shown in previous studies (*23*, *24*, *34*, *35*), but this strategy cannot be directly applied to our system owing to the complexity of hierarchical composite nanoporous systems.

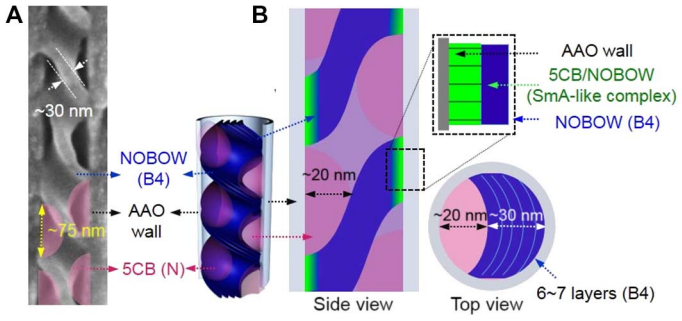

Fig. 4. Schemes of 5CB/NOBOW ordering confined in chiral nanopores. (**A**) Dimensional measurement of helical voids generated in between the AAO wall and pretransitioned HNF backbone when used as the channels (d_{AAO} = 60 nm). (**B**) Configuration of the smectic A (SmA)–like ordering of 5CB confined in AAO/HNF.

CONCLUSION

In conclusion, we reported a new LC phase behavior from the conventional nematic LC molecules. The fluid-like nematic LC phase exhibited an unprecedentedly high positional and orientational order under multiple spatial confinements by being introduced with bent-core LC molecules in a confined geometry. The 5CB molecules were placed in an extremely limited space (that is, facing the two different interfaces with preformed vertical HNFs and the oxide wall from the AAO channels) while they had to maintain specific interfacial interactions to the given surfaces. These conditions limited the molecular organization into the smectic-like ordering in the regularly generated helical voids. This dual-confining system produced a highly ordered nematic LC phase and can suggest new research areas for nondisplay applications, such as chiral separation, chirality detection, and 3D nanopatterning application.

MATERIALS AND METHODS

Sample preparation

1D nanochannels (AAO films) were electrochemically synthesized with the fixed dimension of the pores (60 nm) with the fixed depth (L = 5 and 100 μm) by the two-step anodization method based on previous studies (*36*, *37*). A binary mixture of NOBOW and 5CB was prepared by simple mixing at isotropic temperature (185°C), and its mixing ratio was quantitatively varied on the basis of its weight fraction (*2*). Their uniform miscibility was preconfirmed by polarized optical microscopy (POM) after (fig. S1; 5°C/min). Then, the mixtures were introduced onto the top of prepared nanochannels by simply increasing the surface temperature up to that of isotropic phase (185°C). The samples at isotropic melt state were slowly cooled down to 110°C, where the mixtures were rather fluidic but strongly anchored by the channel wall. During this stage, residual bulk mixture on top of the film was removed by gentle wiping with tips, with the result that only nanoconfined mixture could be obtained without the bulk information.

EM imaging analysis

For SEM study, small fragments of AAO films (~2 mm × ~5 mm) containing NOBOW-5CB mixture were prepared at room temperature after finishing the whole thermal transitions of both molecules. Before the EM imaging, the samples were dropped into EtOH for 5 min for selective removal of 5CB. Then, the films were gently bent from both ends to make the cracks at the surface, and a cross-sectional view of nanoconfined HNF templates was exposed. Next, the samples were coated with a 3-nm-thick layer of platinum to minimize electron beam damage on the sample. For direct TEM imaging, after EtOH washing, the individual nanoconfined HNFs were isolated from AAO channels by dissolving aluminum oxide wall in 0.1 M NaOH solution for 1 hour. Released individual HNFs were collected by dropping onto the TEM grid (carbon-supported, 300 meshes). All the resulting EM images (Fig. 3 and figs. S2 to S4) of nanoconfined HNFs were acquired at high-ordered B4 state (at 25°C).

In situ GIXD analysis

All GIXD experiments were performed in 9A (Ultra-SAXS beamline) at PLS-II (Pohang Light Source–II) in Pohang, Korea. All the samples were prepared with the square type (10-mm × 10-mm area) without residual bulk samples on top of the films. The beam size is 70 μm (vertical) × 300 μm (horizontal) with an energy of 11.08 keV. Sample-to-detector distance was 235 mm. To investigate the in situ molecular orientation sequences during phase transition from 190° to 25°C, we conducted the GIXD experiment with temperature changes and with a cooling rate of 10°C/min.

SUPPLEMENTARY MATERIALS

Supplementary material for this article is available at http://advances.sciencemag.org/cgi/content/full/3/2/e1602102/DC1

fig. S1. POM images of NOBOW/5CB binary mixtures with the different mixing ratio.

fig. S2. SEM observation on the morphological changes of 5CB/NOBOW mixtures in AAO (d_{AAO} = 60 nm) over the various mixing ratio.

fig. S3. SEM observation on the self-generated chiral porous nanostructures from pure NOBOW.

fig. S4. Geometry of in situ GIXD measurement for the simultaneous investigation of the molecular orientation and layer arrangement over the whole thermal LC phase transition.

fig. S5. Solvent damage tests on the HNF morphology with EtOH.

fig. S6. Contact angle measurement to quantitatively confirm the relative mutual interaction forces with the various interfacial conditions.

fig. S7. 2D GIXD patterns comparing the pure 5CB and 8CB confined in AAO nanochannels (d_{AAO} = 60 nm).

fig. S8. GIXD and SEM observations to confirm the optimal range of the spatial dimension of AAO for the successful confinement of 5CB/NOBOW mixture.

REFERENCES AND NOTES

1. L. E. Hough, H. T. Jung, D. Krüerke, M. S. Heberling, M. Nakata, C. D. Jones, D. Chen, D. R. Link, J. Zasadzinski, G. Heppke, J. P. Rabe, W. Stocker, E. Körblova, D. M. Walba, M. A. Glaser, N. A. Clark, Helical nanofilament phases. *Science* **325**, 456–460 (2009).
2. D. Chen, J. E. Maclennan, R. Shao, D. K. Yoon, H. Wang, E. Korblova, D. M. Walba, M. A. Glaser, N. A. Clark, Chirality-preserving growth of helical filaments in the B4 phase of bent-core liquid crystals. *J. Am. Chem. Soc.* **133**, 12656–12663 (2011).
3. T. Sekine, T. Niori, J. Watanabe, T. Furukawa, S. W. Choi, H. Takezoe, Spontaneous helix formation in smectic liquid crystals comprisingachiral molecules. *J. Mater. Chem.* **7**, 1307–1309 (1997).
4. K. Yamada, S. Kang, K. Takimoto, M. Hattori, K. Shirata, S. Kawauchi, K. Deguchi, T. Shimizu, J. Watanabe, Structural analysis of a banana-liquid crystal in the B4 phase by solid-state NMR. *J. Phys. Chem. B* **117**, 6830–6838 (2013).
5. C. Zhu, C. Wang, A. Young, F. Liu, I. Gunkel, D. Chen, D. Walba, J. Maclennan, N. Clark, A. Hexemer, Probing and controlling liquid crystal helical nanofilaments. *Nano Lett.* **15**, 3420–3424 (2015).
6. C. Zhang, N. Diorio, O. D. Lavrentovich, A. Jákli, Helical nanofilaments of bent-core liquid crystals with a second twist. *Nat. Commun.* **5**, 3302 (2014).
7. H. Kim, S. Lee, T. J. Shin, E. Korblova, D. M. Walba, N. A. Clarke, S. B. Lee, D. K. Yoon, Multistep hierarchical self-assembly of chiral nanopore arrays. *Proc. Natl. Acad. Sci. U.S.A.* **111**, 14342–14347 (2014).
8. H. Kim, A. Zep, S. H. Ryu, H. Ahn, T. J. Shin, S. B. Lee, D. Pociecha, E. Gorecka, D. K. Yoon, Linkage-length dependent structuring behavior of bent-core molecules in helical nanostructures. *Soft Matter* **12**, 3326–3330 (2016)
9. R. Zhang, X. Zeng, B. Kim, R. J. Bushby, K. Shin, P. J. Baker, V. Percec, P. Leowanawat, G. Ungar, Columnar liquid crystals in cylindrical nanoconfinement. *ACS Nano* **9**, 1759–1766 (2015).
10. R. Zhang, X. Zeng, M. Prehm, F. Liu, S. Grimm, M. Geuss, M. Steinhart, C. Tschierske, G. Ungar, Honeycombs in honeycombs: Complex liquid crystal alumina composite mesostructures. *ACS Nano* **8**, 4500–4509 (2014).
11. Y. Wu, G. Cheng, K. Katsov, S. W. Sides, J. Wang, J. Tang, G. H. Fredrickson, M. Moskovits, G. D. Stucky, Composite mesostructures by nano-confinement. *Nat. Mater.* **3**, 816–822 (2004).
12. S. H. Ryu, D. K. Yoon, Liquid crystal phases in confined geometries. *Liq. Cryst.* **43**, 13–15 (2016).
13. T.-T. Tang, C.-Y. Kuo, R.-P. Pan, J.-M. Shieh, C.-L. Pan, Strong vertical alignment of liquid crystal on porous anodic aluminum oxide film. *J. Disp. Technol.* **5**, 350–354 (2009).
14. C. Chen, P. J. Bos, J. E. Anderson, Anchoring transitions of liquid crystals on SiO_x. *Liq. Cryst.* **35**, 465–481 (2008).
15. R. J. Ondris-Crawford, G. P. Crawford, S. Zumer, J. W. Doane, Curvature-induced configuration transition in confined nematic liquid crystals. *Phys. Rev. Lett.* **70**, 194 (1993).
16. C. Grigoriadis, H. Duran, M. Steinhart, M. Kappl, H.-J. Butt, G. Floudas, Suppression of phase transitions in a confined rodlike liquid crystal. *ACS Nano* **5**, 9208–9215 (2011).
17. E. Lacaze, M. Alba, M. Goldmann, J. P. Michel, F. Rieutord, Dimerization in the commensurate network of 4-*n*-octyl-4′-cyanobiphenyl (8CB) molecules adsorbed on MoS_2 single crystal. *Eur. Phys. J. B.* **39**, 261–272 (2004).
18. P. Kędzioraa, J. Jadzyna, Dimerization of polar mesogenic molecules. *Mol. Cryst. Liq. Cryst. Inc. Nonlinear Opt.* **192**, 31–37 (2006).
19. C. Zhu, D. Chen, Y. Shen, C. D. Jones, M. A. Glaser, J. E. Maclennan, N. A. Clark, Nanophase segregation in binary mixtures of a bent-core and a rodlike liquid-crystal molecule. *Phys. Rev. E* **81**, 011704 (2010).
20. H. Nagayama, Y. Sasaki, F. Araoka, K. Ema, K. Ishikawa, H. Takezoe, Discrete and sequential formation of helical nanofilaments in mixtures consisting of bent- and rod-shaped molecules. *Soft Matter* **7**, 8766–8769 (2011).
21. D. Chen, C. Zhu, R. K. Shoemaker, E. Korblova, D. M. Walba, M. A. Glaser, J. E. Maclennan, N. A. Clark, Pretransitional orientational ordering of a calamitic liquid crystal by helical nanofilaments of a bent-core mesogen. *Langmuir* **26**, 15541–15545 (2010).
22. Y. Takanishi, G. J. Shin, J. C. Jung, S.-W. Choi, K. Ishikawa, J. Watanabe, H. Takezoe, P. Toledano, Observation of very large chiral domains in a liquid crystal phase formed by mixtures of achiral bent-core and rod molecules. *J. Mater. Chem.* **15**, 4020–4024 (2005).
23. Y. S. Touloukian, D. P. DeWitt, *Thermophysical Properties of Matter* (Springer, 1970).
24. D. Chen, M. R. Tuchband, B. Horanyi, E. Korblova, D. M. Walba, M. A. Glaser, J. E. Maclennan, N. A. Clark, Diastereomeric liquid crystal domains at the mesoscale. *Nat. Commun.* **6**, 7763 (2015).
25. Y. Takanishi, H. Yao, T. Fukasawa, K. Ema, Y. Ohtsuka, Y. Takahashi, J. Yamamoto, H. Takezoe, A. Iida, Local orientational analysis of helical filaments and nematic director in

a nanoscale phase separation composed of rod-like and bent-core liquid crystals using small- and wide-angle X-ray microbeam scattering. *J. Phys. Chem. B* **118**, 3998–4004 (2014).
26. P. Ziherl, M. Vilfan, N. Vrbančič-Kopač, S. Žumer, R. J. Ondris-Crawford, G. P. Crawford, Substrate-induced order in the isotropic phase of a smectogenic liquid crystal: A deuteron NMR study. *Phys. Rev. E* **61**, 2792 (2000).
27. M. P. Valignat, S. Villette, J. Li, R. Barberi, R. Bartolino, E. Dubois-Violette, A. M. Cazabat, Wetting and anchoring of a nematic liquid crystal on a rough surface. *Phys. Rev. Lett.* **77**, 1994–1997 (1996).
28. C. Poulard, M. Voué, J. D. Coninck, A. M. Cazabat, Spreading of nematic liquid crystals on hydrophobic substrates. *Colloid. Surface A* **282–283**, 240–246 (2006).
29. W. Iglesias, T. J. Smith, P. B. Basnet, C. Tschierske, D. J. Lacks, A. Jakli, E. K. Mann, Alignment by Langmuir/Schaefer monolayers of bent-core liquid crystals. *Soft Matter* **7**, 9043–9050 (2011).
30. O. D. Lavrentovich, Topological defects in dispersed words and worlds around liquid crystals, or liquid crystal drops. *Liq. Cryst.* **24**, 117–126 (1998).
31. E. I. Givargizov, *Oriented Crystallization on Amorphous Substrates* (Springer Science + Business Media, 1991).
32. D. W. Berreman, Solid surface shape and the alignment of an adjacent nematic liquid crystal. *Phys. Rev. Lett.* **28**, 1683–1686 (1972).
33. A. Buka, *Modern Topics in Liquid Crystals: From Neutron Scattering to Ferroelectricity* (World Scientific Publishing Co., 1993).
34. T. Otani, F. Araoka, K. Ishikawa, H. Takezoe, Enhanced optical activity by achiral rod-like molecules nanosegregated in the B_4 structure of achiral bent-core molecules. *J. Am. Chem. Soc.* **131**, 12368–12372 (2009).
35. K. Kim, H. Kim, S.-Y. Jo, F. Araoka, D. K. Yoon, S.-W. Choi, Photomodulated supramolecular chirality in achiral photoresponsive rodlike compounds nanosegregated from the helical nanofilaments of achiral bent-core molecules. *ACS Appl. Mater. Interfaces* **7**, 22686–22691 (2015).
36. C. R. Martin, Nanomaterials: A membrane-based synthetic approach. *Science* **266**, 1961–1966 (1994).
37. A. P. Li, F. Müller, A. Birner, K. Nielsch, U. Gösele, Hexagonal pore arrays with a 50–420 nm interpore distance formed by self-organization in anodic alumina. *J. Appl. Phys.* **84**, 6023–6026 (1998).

Acknowledgments
Funding: This work was supported by the National Research Foundation, funded by the Korean Government Ministry of Science, ICT and Future Planing (MSIP) (grant 2014M3C1A3052537), Ministry of Education (MOE) (grant 2014S1A2A2027911), and by the Materials Research Science and Engineering Center Program funded by NSF (grant DMR-1420736). Experiments at the PLS-II were supported in part by MSIP and Pohang University of Science and Technology. **Author contributions:** H.K. and D.K.Y. designed the research. H.K., S.H.R., and T.J.S. performed the research. M.T., E.K., and D.M.W. contributed new reagents/analytic tools. H.K., D.M.W., N.A.C., and D.K.Y. analyzed the data. H.K., D.M.W., N.A.C., and D.K.Y. wrote the paper. **Competing interests:** D.K.Y. has a patent related to the work, 10-2014-0093515. The other authors declare that they have no competing interests. **Data and materials availability:** All data needed to evaluate the conclusions in the paper are present in the paper and/or the Supplementary Materials. Additional data related to this paper may be requested from the authors.

Submitted 2 September 2016
Accepted 21 December 2016
Published 10 February 2017
10.1126/sciadv.1602102

Citation: H. Kim, S. H. Ryu, M. Tuchband, T. J. Shin, E. Korblova, D. M. Walba, N. A. Clark, D. K. Yoon, Structural transitions and guest/host complexing of liquid crystal helical nanofilaments induced by nanoconfinement. *Sci. Adv.* **3**, e1602102 (2017).

Structural transitions and guest/host complexing of liquid crystal helical nanofilaments induced by nanoconfinement

Hanim Kim, Seong Ho Ryu, Michael Tuchband, Tae Joo Shin, Eva Korblova, David M. Walba, Noel A. Clark and Dong Ki Yoon

Sci Adv **3** (2), e1602102.
DOI: 10.1126/sciadv.1602102